energies

MDPI

Article

Minimizing Leakage Magnetic Field of Wireless Power Transfer Systems Using Phase Difference Control

Seongho Woo [1], Yujun Shin [1], Changmin Lee [1], Jaewon Rhee [1], Jangyong Ahn [1], Jungick Moon [2], Seokhyeon Son [3], Sanguk Lee [1], Hongseok Kim [1] and Seungyoung Ahn [1,*]

[1] Cho Chun Shik Graduate School of Mobility, Korea Advanced Institute of Science and Technology, Daejeon 34051, Korea
[2] Electronics and Telecommunications Research Institute, Daejeon 34129, Korea
[3] Hyundai Motors, 40, Namyang 18270, Korea
* Correspondence: sahn@kaist.ac.kr

Abstract: In this paper, we propose a method to reduce the leakage magnetic field from wireless power transfer (WPT) systems with series–series compensation topology by adjusting the phase difference between the transmitter (TX) coil current and the receiver (RX) coil current without additional shielding coils or materials. A WPT system employing the proposed method adjusts the phase difference between the TX coil current and RX coil current by tuning a resonant capacitor of the RX coil. The conditions for minimizing the leakage magnetic field are derived, and the range of the resonant capacitor of RX, considering power transfer efficiency and the leakage magnetic field, is proposed. Through simulations and experiments, it is verified that the proposed method can reduce the leakage magnetic field level without any additional materials. For that reason, the proposed method can be suitable for size-limited, weight-limited or cost-limited WPT systems.

Keywords: wireless power transfer (WPT); leakage magnetic field; electromagnetic field (EMF); shielding method

Citation: Woo, S.; Shin, Y.; Lee, C.; Rhee, J.; Ahn, J.; Moon, J.; Son, S.; Lee, S.; Kim, H.; Ahn, S. Minimizing Leakage Magnetic Field of Wireless Power Transfer Systems Using Phase Difference Control. *Energies* **2022**, *15*, 8202. https://doi.org/10.3390/en15218202

Academic Editor: Alon Kuperman

Received: 28 September 2022
Accepted: 31 October 2022
Published: 3 November 2022

1. Introduction

Wireless power transfer (WPT) technology is an attractive solution for replacing wired charging because of its convenience, safety, etc. [1–3]. Since the advent of WPT technology, it has been used in many applications, such as low-power and high-power applications. The WPT technology for smartwatches and smartphones is already commercialized [4,5], and WPT technology for unmanned vehicles such as AGVs and drones is being actively studied. Moreover, as the demand for electric vehicles (EVs) increases, WPT technology has received more and more attention.

WPT technology uses a magnetic field to transfer power from the transmitter (TX) to the receiver (RX). During the process of transferring power, coupled and leakage magnetic fields are produced, as shown in Figure 1. The leakage magnetic field affects the human body and other electronic devices. Usually, the term used for human effects is electromagnetic field (EMF), and the term used for effects on other electronic devices is electromagnetic interference (EMI) [6,7]. For the commercialization of the WPT system, it is necessary to solve the EMF/EMI problem. Thus, many studies are being conducted to solve these problems.

In general, the shielding methods can be classified into four types, as shown in Figure 2. First, the metallic shielding method [8] uses conductive material. When the magnetic field is induced in the conductive material, the eddy current generates a magnetic field opposite to the magnetic field generated by the TX or RX coils. The disadvantages of this method are that the power transfer efficiency (PTE) may be reduced, and the weight and cost of the WPT system may be increased. Second, the magnetic shielding method [9] uses magnetic material that has high permeability. The magnetic material has a lower reluctance than

that of air, so the magnetic field generated by the TX or RX coils can be guided through the magnetic material. This method also has disadvantages, in that the weight and cost of the WPT system may be increased. Furthermore, as the power level increases, the current flowing into TX and RX coils can be increased. As a result, the magnetic material can become saturated. Third, the active shielding method uses an additional coil and power source [10] to generate a magnetic field opposite to the magnetic field generated by the TX and RX coils. When using this method, the complexity of the system may be increased, and the PTE may be lowered. Finally, the reactive shielding method [11] uses an additional coil. When the voltage is induced at the shielding coil by the magnetic field generated by TX or RX coils, then controlling the phase of the shielding (SH) coil impedance by tuning the matching capacitor of the SH coil cancels the magnetic field generated by TX or RX coils. Because an additional power source is not needed and the shielding performance is high, the reactive shielding method is a promising technology that can be used in various applications. Besides the above methods, there are methods to add a filter for controlling the impedance [12,13].

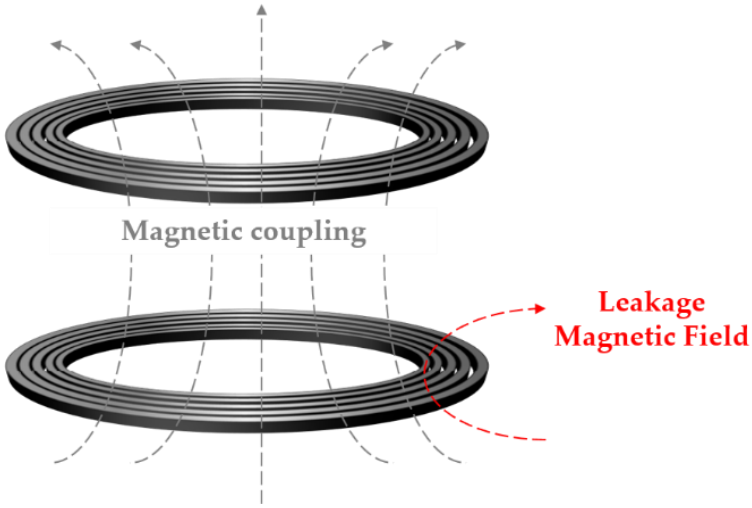

Figure 1. Coupled and leakage magnetic field in the process of transferring power wirelessly.

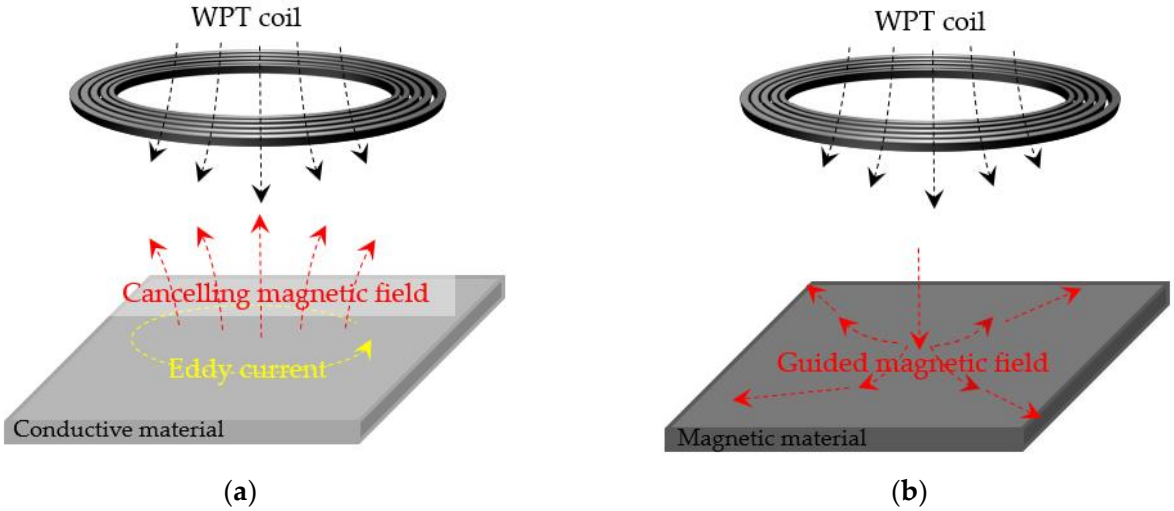

(**a**) (**b**)

Figure 2. *Cont.*

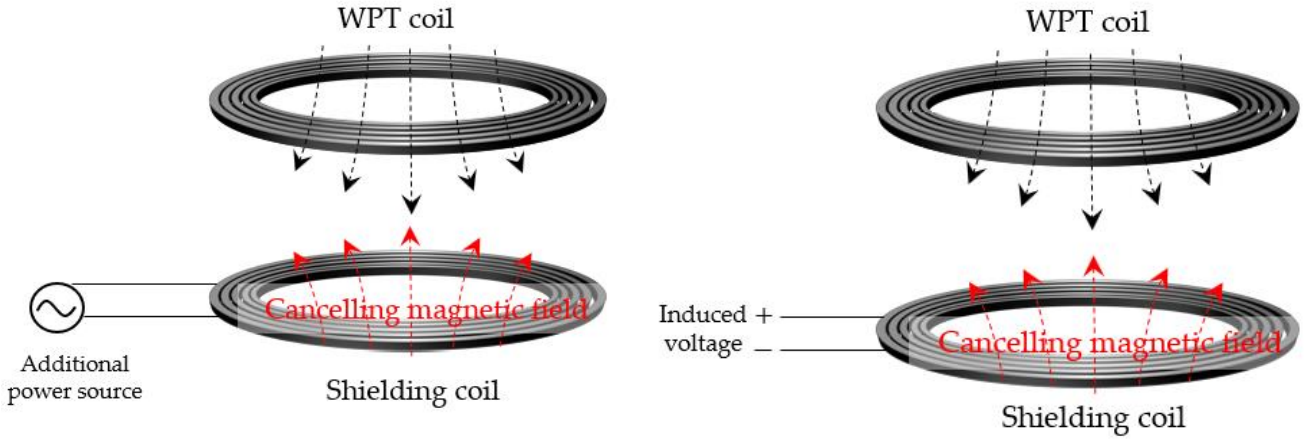

Figure 2. Various shielding methods used in WPT System: (**a**) metallic shielding; (**b**) magnetic shielding; (**c**) active shielding; (**d**) reactive shielding.

However, all existing methods need additional materials, such as conductive material, magnetic material, coils, or power sources, and as a result, the size, weight or the cost of the WPT system can be increased. Not using additional materials is necessary to reduce the size, weight, and cost of the WPT system.

In this paper, we will propose a method for minimizing the leakage magnetic field through phase difference control between TX coil current and RX coil current, without using additional materials.

The contributions of this paper are as follows:

(1) The proposed WPT system can minimize the leakage magnetic field without additional materials, power sources or coils. Thus, the proposed method can reduce the size, weight and cost of the WPT system.

(2) The previous research related to WPT systems only focus on resonant systems to maximize the power transfer efficiency (PTE) and power transfer capacity (PTC). This paper focuses on resonant systems in terms of the leakage magnetic field while also considering the PTE and PTC.

This paper is arranged as follows: In Section 2, the minimization method of leakage magnetic field of the WPT system is presented. In Section 3, we verify the proposed method through simulation and experiment. Finally, in Section 4, we conclude our research.

2. Minimization Method of Leakage Magnetic Field of Wireless Power Transfer System

2.1. Method of Phase Difference Control between TX Coil Current and RX Coil Current

We will explain how to control the phase difference between TX coil current and RX coil current. Figure 3 shows the leakage magnetic field generated by TX or RX coils. When the TX and RX currents flow into the coils, the magnetic field is generated, and the magnetic field strength is the function of turn, current, and the distance from coils, as expressed in Equation (1).

$$|\mathbf{B_{total}}| = |\mathbf{B_{TX}} + \mathbf{B_{RX}}| \propto \left| \frac{N_{TX}\mathbf{I_{TX}}}{{d_{TX}}^3} + \frac{N_{RX}\mathbf{I_{RX}}}{{d_{RX}}^3} \right| \quad (1)$$

where N_{TX} and N_{RX} are the turns of the TX coil and RX coil, $\mathbf{I_{TX}}$ and $\mathbf{I_{RX}}$ are the TX coil current and RX coil current, and d_{TX} and d_{RX} are the distance between the observation point and the center of each coil. First, we should derive the relationship between $\mathbf{I_{TX}}$ and $\mathbf{I_{RX}}$ to express the phase difference between $\mathbf{I_{TX}}$ and $\mathbf{I_{RX}}$.

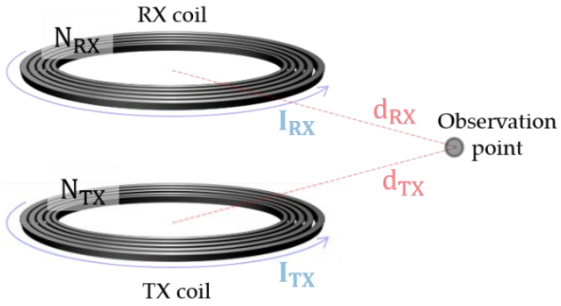

Figure 3. The magnetic field strength generated by the TX coil and RX coil.

Figure 4 shows the equivalent circuit of the series–series compensation topology of the WPT system. When applying the KVL in the RX part, $\mathbf{I_{RX}}$ can be expressed as in Equation (2).

$$\mathbf{I_{RX}}=\frac{-j\omega_o M_{TX-RX}}{R_{RX}+R_L+jX_{RX}}\mathbf{I_{TX}} \cong \frac{-j\omega_o M_{TX-RX}}{R_L+jX_{RX}}\mathbf{I_{TX}}=\frac{\omega_o M_{TX-RX}}{\sqrt{{R_L}^2+{X_{RX}}^2}}I_{TX}\angle\left(-\frac{\pi}{2}-tan^{-1}\frac{X_{RX}}{R_L}\right) \quad (2)$$

where ω_o is the operating frequency of the WPT system, and X_{RX} is the reactance component of RX part whose value is $\frac{{\omega_o}^2 L_{RX}C_{RX}-1}{\omega_o C_{RX}}$. Depending on X_{RX}, the phase difference between $\mathbf{I_{TX}}$ and $\mathbf{I_{RX}}$ can be controlled. The phases of $\mathbf{B_{TX}}$ and $\mathbf{B_{RX}}$ are determined by $\mathbf{I_{TX}}$ and $\mathbf{I_{RX}}$; thus, the phase difference between $\mathbf{B_{TX}}$ and $\mathbf{B_{RX}}$ is equal to the phase difference between $\mathbf{I_{TX}}$ and $\mathbf{I_{RX}}$ as shown in Figure 5. Figure 5 shows the various cases for the operating frequency and phase difference between $\mathbf{I_{TX}}$ ($\mathbf{B_{TX}}$) and $\mathbf{I_{RX}}$ ($\mathbf{B_{RX}}$). As shown in Figure 5a, when the resonant frequency of RX (ω_{RX}) and the operating frequency (ω_o) are the same, the phase difference between $\mathbf{I_{TX}}$ ($\mathbf{B_{TX}}$) and $\mathbf{I_{RX}}$ ($\mathbf{B_{RX}}$) is $\frac{\pi}{2}$, and as shown in Figure 5b, when ω_{RX} has a larger value than ω_o, the phase difference between $\mathbf{I_{TX}}$ ($\mathbf{B_{TX}}$) and $\mathbf{I_{RX}}$ ($\mathbf{B_{RX}}$) is $0 \sim \frac{\pi}{2}$. Additionally, as shown in Figure 5c, when ω_{RX} has a lower value than ω_o, the phase difference between $\mathbf{I_{TX}}$ ($\mathbf{B_{TX}}$) and $\mathbf{I_{RX}}$ ($\mathbf{B_{RX}}$) is $\frac{\pi}{2} \sim \pi$.

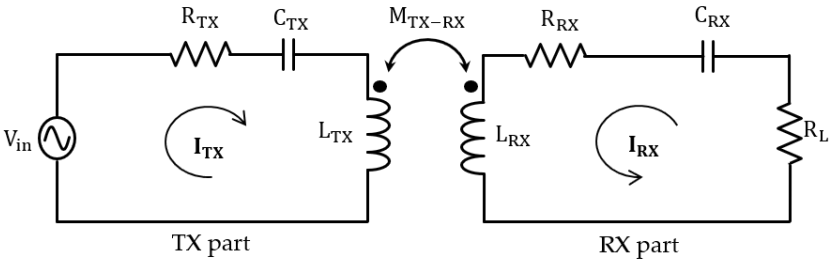

Figure 4. The equivalent circuit of series–series compensation topology of the WPT system.

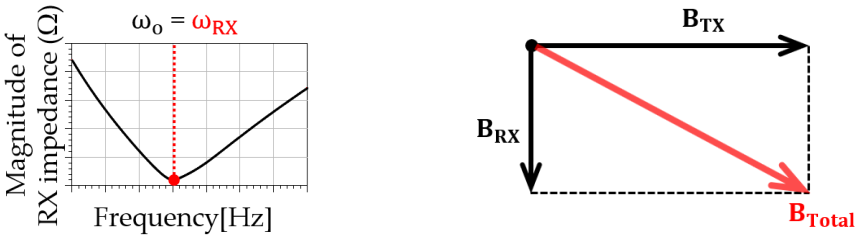

(**a**)

Figure 5. *Cont.*

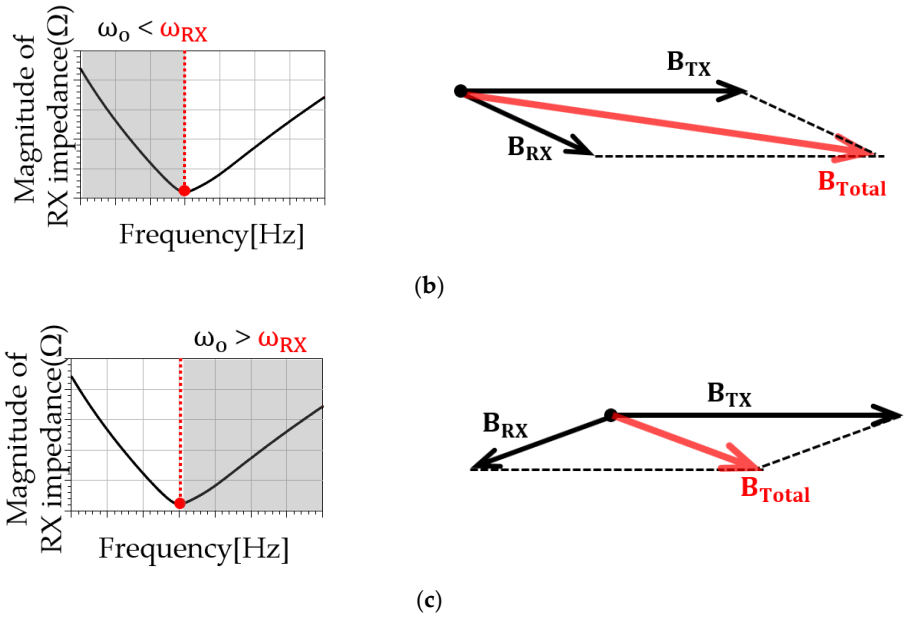

Figure 5. Various cases for the magnitude of RX part impedance and vector diagram of $\mathbf{I_{TX}}$($\mathbf{B_{TX}}$) and $\mathbf{I_{RX}}$($\mathbf{B_{RX}}$) depending on ω_{RX} and ω_o: (**a**) $\omega_{RX} = \omega_o$; (**b**) $\omega_{RX} > \omega_o$; (**c**) $\omega_{RX} < \omega_o$.

In summary, controlling the phase difference between $\mathbf{I_{TX}}$ ($\mathbf{B_{TX}}$) and $\mathbf{I_{RX}}$ ($\mathbf{B_{RX}}$) can be possible through tuning ω_{RX}.

2.2. Minimization Condition of Leakage Magnetic Field of WPT System and Its Performances

The minimization condition of leakage magnetic field in the WPT system and the performance parameters such as power transfer efficiency (PTE) and power transfer capacity (PTC) will be explained in detail.

First, we decide the region of ω_{RX}. To reduce the leakage magnetic field, ω_{RX} has a lower value than ω_o, i.e., the phase difference between $\mathbf{I_{TX}}$ ($\mathbf{B_{TX}}$) and $\mathbf{I_{RX}}$ ($\mathbf{B_{RX}}$) should be $\frac{\pi}{2} \sim \pi$. For calculations of the total magnetic field strength, we should express the term $\mathbf{I_{TX}}$ into $\mathbf{I_{RX}}$. $\mathbf{I_{RX}}$ is expressed as in Equation (3).

$$\mathbf{I_{RX}} = I_{RX}\angle\left(-\frac{\pi}{2} - tan^{-1}\frac{X_{RX}}{R_L}\right) \tag{3}$$

To compare the leakage magnetic field with the same output power, we assume the I_{RX} has the constant value, as in Equation (4).

$$P_{out} = {I_{RX}}^2 R_L, \ \frac{\partial I_{RX}}{\partial X_{RX}} = 0 \tag{4}$$

where P_{out} and R_L are the desired values of the WPT system.

After assuming $\mathbf{I_{RX}}$ as in Equation (3), $\mathbf{I_{TX}}$ can be calculated as in Equation (5).

$$\mathbf{I_{TX}} = \frac{\sqrt{{R_L}^2 + {X_{RX}}^2}}{\omega_o M_{TX-RX}} I_{RX}\angle 0 \tag{5}$$

As a result, the total magnetic field in Equation (1) can be calculated as in Equation (6).

$$\begin{gathered} |\,\mathbf{B_{total}}\,| \propto \left|\,\frac{N_{TX}\mathbf{I_{TX}}}{{d_{TX}}^3} + \frac{N_{RX}\mathbf{I_{RX}}}{{d_{RX}}^3}\,\right| = \\ \left|\,\frac{N_{TX}}{{d_{TX}}^3}\frac{\sqrt{{R_L}^2+{X_{RX}}^2}}{\omega_o M_{TX-RX}} I_{RX}\angle 0 + \frac{N_{RX}}{{d_{RX}}^3} I_{RX}\angle\left(-\frac{\pi}{2} - tan^{-1}\frac{X_{RX}}{R_L}\right)\right| = F \end{gathered} \tag{6}$$

When we define the magnitude of the magnetic field F, we can express the vector diagram as in Figure 6. Moreover, we can calculate F^2 using the law of cosines as in Equation (7).

$$F^2 = {I_{RX}}^2 \left(\frac{{N_{TX}}^2}{{d_{TX}}^6} \frac{{X_{RX}}^2 + {R_L}^2}{{\omega_o}^2 {M_{TX-RX}}^2} + \frac{{N_{RX}}^2}{{d_{RX}}^6} - 2\frac{N_{TX} N_{RX}}{{d_{TX}}^3 {d_{RX}}^3} \frac{X_{RX}}{\omega_o M_{TX-RX}} \right) \tag{7}$$

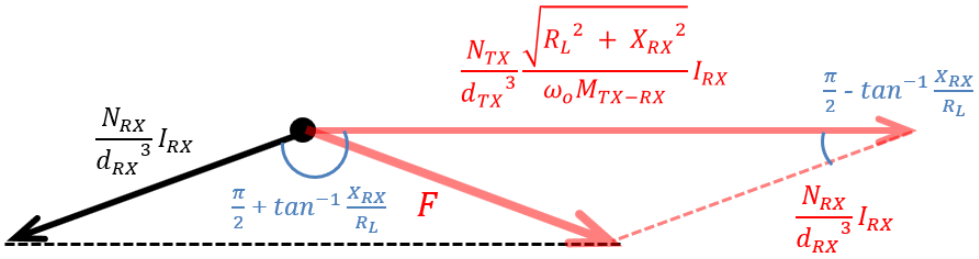

Figure 6. The vector diagram in Equation (6).

The variable X_{RX}, which becomes 0 when F^2 is differentiated with respect to X_{RX}, is the value for minimizing the leakage magnetic field, expressed in Equation (8).

As shown in Equation (8), the minimization condition of the leakage magnetic field can be determined by N_{TX} and N_{RX}, d_{TX} and d_{RX}, ω_o, and the mutual inductance between the TX coil and RX coil (M_{TX-RX}).

$$\begin{gathered} \frac{dF^2}{dX_{RX}} = {I_{RX}}^2 \left(2\frac{{N_{TX}}^2}{{d_{TX}}^6} \frac{X_{RX}}{{\omega_o}^2 {M_{TX-RX}}^2} - 2\frac{N_{TX} N_{RX}}{{d_{TX}}^3 {d_{RX}}^3} \frac{1}{\omega_o M_{TX-RX}} \right) = 0, \\ X_{RX} = \frac{N_{RX}}{N_{TX}} \left(\frac{d_{TX}}{d_{RX}} \right)^3 \omega_o M_{TX-RX} \end{gathered} \tag{8}$$

However, when X_{RX} exceeds some value, the leakage magnetic field increases compared to the conventional WPT system. Therefore, we should decide the range of X_{RX}. As shown in Equation (7), F^2 is the quadratic function of X_{RX}. So, when solving the Equation (9), we can find the range of X_{RX} value, and the range of X_{RX} can be expressed as in Equation (10).

$$\mathrm{F}^2 \big|_{X_{RX}=0} = \mathrm{F}^2 \big|_{X_{RX}=X}, \; X = 2\frac{N_{RX}}{N_{TX}} \left(\frac{d_{TX}}{d_{RX}} \right)^3 \omega_o M_{TX-RX} \tag{9}$$

$$0 \le X_{RX} \le 2\frac{N_{RX}}{N_{TX}} \left(\frac{d_{TX}}{d_{RX}} \right)^3 \omega_o M_{TX-RX} \tag{10}$$

In Equation (10), when X_{RX} is equal to zero, this can be understood as a conventional WPT system.

The conceptual diagram of the proposed method is shown in Figure 7. Expressed as in Equations (3) and (4), the magnitude of $\mathbf{I_{RX}}$, I_{RX} is the constant value for the same output power, and the phase of $\mathbf{I_{RX}}$, $-\frac{\pi}{2} - tan^{-1} \frac{X_{RX}}{R_L}$ can be adjustable with the range $[-\pi, -\frac{\pi}{2}]$, depending on the value of X_{RX}. And as expressed in Equation (5), the magnitude of $\mathbf{I_{TX}}$, $\frac{\sqrt{{R_L}^2 + {X_{RX}}^2}}{\omega_o M_{TX-RX}} I_{RX}$, increases as the value of X_{RX} increases, and the phase of $\mathbf{I_{TX}}$ is 0 because we assume that the phase of $\mathbf{I_{TX}}$ is the reference angle.

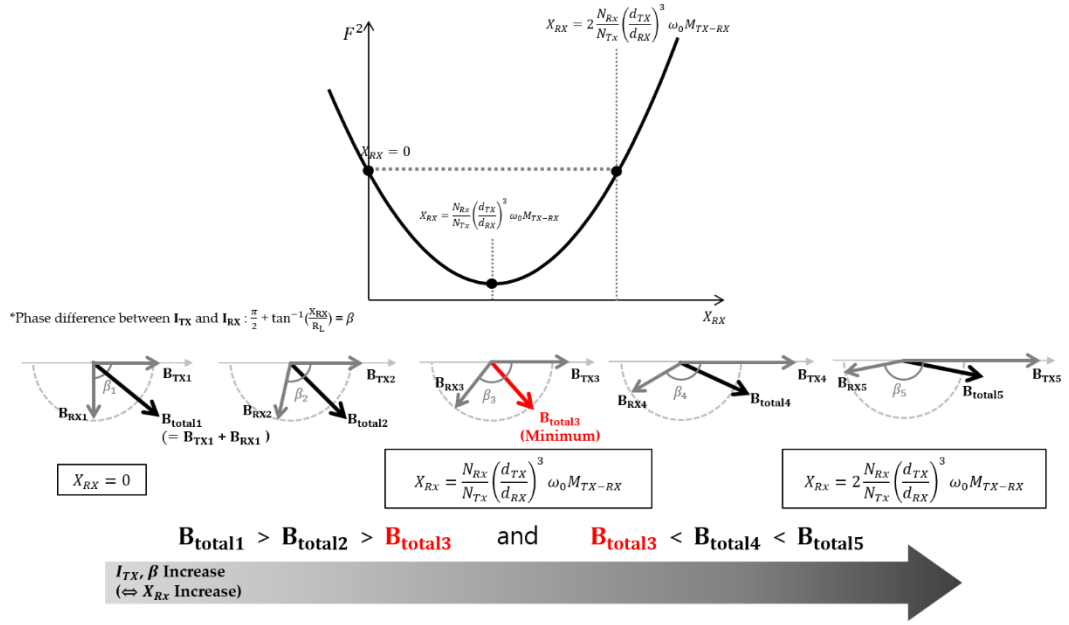

Figure 7. The conceptual diagram of the proposed method.

As shown in Figure 7, when X_{RX} is equal to $\frac{N_{RX}}{N_{TX}}\left(\frac{d_{TX}}{d_{RX}}\right)^3 \omega_o M_{TX-RX}$, the leakage magnetic field of the WPT system can be minimized.

Meanwhile, when the reactance component exists, the PTE decreases. In Figure 4, the PTE is defined as the ratio of the input power and the output power, and can be calculated as in Equation (11).

$$\text{PTE } (\eta) = \frac{\omega_o{}^2 M_{TX-RX}{}^2 R_L}{R_{TX}(X_{RX}{}^2 + (R_{RX} + R_L)^2) + \omega_o{}^2 M_{TX-RX}{}^2 (R_{RX} + R_L)} \tag{11}$$

As X_{RX} increases, the PTE of the WPT system decreases. The leakage magnetic field level and the PTE of the WPT system can be shown in Figure 7.

As shown in Figure 8, the range of Equation (10) should be redefined as Equation (12) because when X_{RX} exceeds $\frac{N_{RX}}{N_{TX}}\left(\frac{d_{TX}}{d_{RX}}\right)^3 \omega_o M_{TX-RX}$, the leakage magnetic field increases and the PTE decreases.

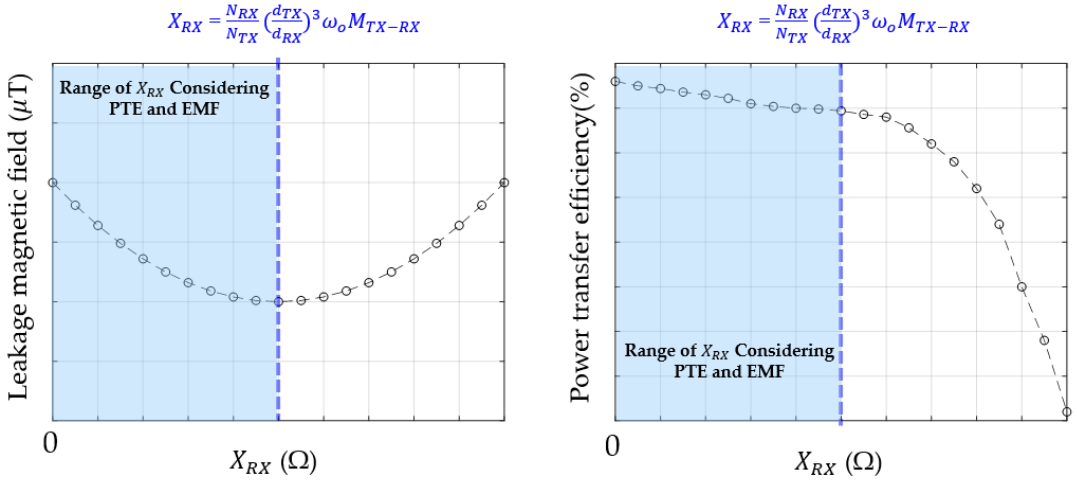

Figure 8. The leakage magnetic field and PTE of the WPT system with changes in X_{RX}.

$$0 \leq X_{RX} \leq \frac{N_{RX}}{N_{TX}}\left(\frac{d_{TX}}{d_{RX}}\right)^3 \omega_o M_{TX-RX} \tag{12}$$

Therefore, by prioritizing, for example, whether the PTE is important or the leakage magnetic field is important, the WPT system can be designed following the range of Equation (12).

In addition, when the reactance component exists, the PTC also decreases. In Figure 4, the PTC is defined as the output power level and calculated as in Equation (13).

$$\text{PTC} = \frac{{\omega_o}^2 {M_{TX-RX}}^2 {V_{in}}^2 R_L}{\left(R_{TX}(R_{RX}+R_L) - X_{TX}X_{RX} + {\omega_o}^2 {M_{TX-RX}}^2\right)^2 + \left(R_{TX}X_{RX} + (R_{RX}+R_L)X_{TX}\right)^2} \tag{13}$$

When X_{TX}= X_{RX}= 0 (conventional WPT system), the PTC (Conv.) can be calculated as in Equation (14).

$$\text{PTC (Conv.)} = \frac{{\omega_o}^2 {M_{TX-RX}}^2 {V_{in,conv}}^2 R_L}{\left(R_{TX}(R_{RX}+R_L)\right)^2} \tag{14}$$

Moreover, when X_{TX}= 0, X_{RX}= X (proposed WPT system), the PTC (Prop.) can be calculated in Equation (15).

$$\text{PTC (Prop.)} = \frac{{\omega_o}^2 {M_{TX-RX}}^2 {V_{in,prop}}^2 R_L}{\left(R_{TX}(R_{RX}+R_L) + {\omega_o}^2 {M_{TX-RX}}^2\right)^2 + \left(R_{TX}\text{X}\right)^2} \tag{15}$$

Therefore, to transfer the same output power when applying the proposed method, the input voltage V_{in} is calculated as in Equation (16).

$$V_{in,prop} = \alpha V_{in,conv}, \alpha = \sqrt{\frac{\left(R_{TX}(R_{RX}+R_L) + {\omega_o}^2 {M_{TX-RX}}^2\right)^2 + \left(R_{TX}\text{X}\right)^2}{\left(R_{TX}(R_{RX}+R_L) + {\omega_o}^2 {M_{TX-RX}}^2\right)^2}} \tag{16}$$

Equation (16) means that when applying the proposed method for the WPT system, the input voltage V_{in} increases by the factor of α.

Table 1 compares the various parameters of conventional and proposed WPT systems. The conventional WPT system has been studied for many years and the characteristics of the conventional WPT system can be referred to [14]. The C_{RX} of the conventional WPT system depends on the operating frequency and L_{RX}, whereas the C_{RX} of the proposed WPT system depends on the operating frequency, L_{RX} and X. The PTE and PTC are at their maximum when employing the conventional WPT system, whereas the EMF is minimized when employing the proposed WPT system.

Table 1. Comparison between the conventional and proposed WPT system.

Parameters	Conventional WPT System	Proposed WPT System
X_{RX}	0	$\frac{N_{RX}}{N_{TX}}\left(\frac{d_{TX}}{d_{RX}}\right)^3 \omega_o M_{TX-RX}$= X
C_{RX}	$\frac{1}{{\omega_o}^2 L_{RX}}$	$\frac{1}{{\omega_o}^2 L_{RX} - \omega_o X}$
PTE	Equation (11) when X_{RX}= 0 (Maximum)	Equation (11) when X_{RX}= X (Less than Conv.)
PTC	Equation (13) when X_{TX}= X_{RX}= 0 (Maximum)	Equation (13) when X_{TX}= 0, X_{RX}= X (Less than Conv.)
EMF	Larger than Prop.	Minimum

In summary, in Section 2.2, we proposed a minimization method for the leakage magnetic field through phase difference control between $\mathbf{I_{TX}}$ and $\mathbf{I_{RX}}$. In addition, we define the range of X_{RX} and analyze the PTE and PTC of the proposed WPT system.

2.3. Consideration of Various Cases—Variations of the Load, Air Gap, and Misalignment

First, we will analyze the variation of the load. Again, the minimization condition of the leakage magnetic field can be expressed as in Equation (17).

$$X_{RX} = \frac{N_{RX}}{N_{TX}} \left(\frac{d_{TX}}{d_{RX}} \right)^3 \omega_o M_{TX-RX} \tag{17}$$

As shown in Equation (17), X_{RX} does not include the term load resistor R_L. The minimization condition of the leakage magnetic field is independent of the load resistor R_L.

Second, we will analyze the variation of the air gap. Figure 9 shows the variations in the air gap between the TX and RX coils. When there is an air gap between the TX and RX coils, the inductance may change [15] because the magnetic or metallic material changes the path of the magnetic field, but we ignore that effect. In this case, we only consider the variations of the mutual inductance (M_{TX-RX}) between the TX and RX coils as the air gap changes. As shown in Equation (16), when the distance between the observation point and each coil is the same and the operating frequency is set, X_{RX} is affected only by M_{TX-RX}. When using the adaptive impedance matching network as explained in [16], X_{RX} can be adjustable.

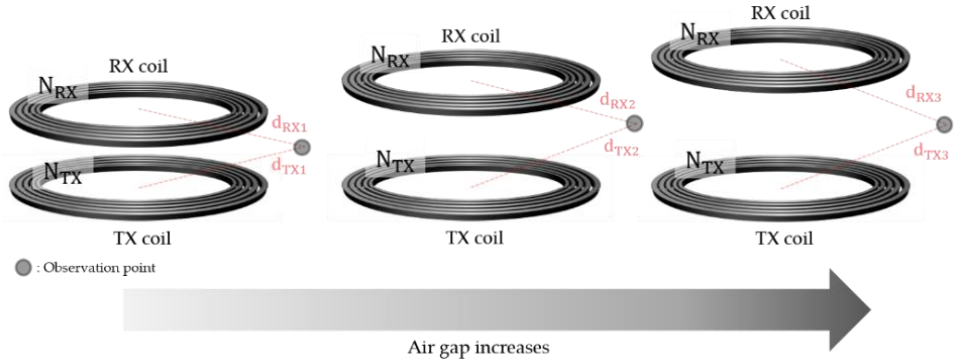

Figure 9. Variations in the air gap between the TX coil and RX coil.

Finally, we will analyze when misalignment occurs. Figure 10 shows the alignment and misalignment cases. When misalignment occurs, the leakage magnetic field increases in the direction of misalignment, and d_{TX} has a larger value than d_{RX}. So, when the operating frequency is set, X_{RX} is affected by $\left(\frac{d_{TX}}{d_{RX}} \right)^3$, M_{TX-RX}. When using the method in [16], X_{RX} can be adjustable also.

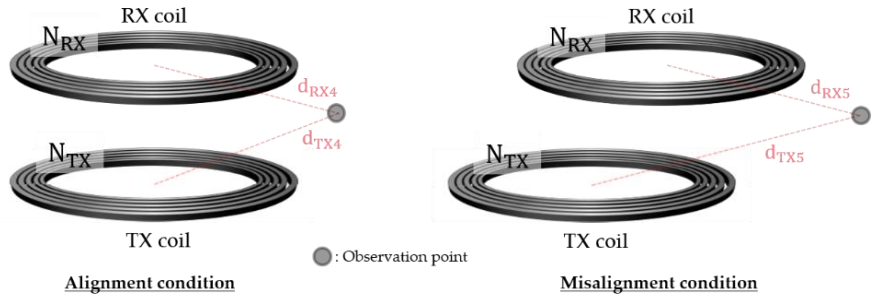

Figure 10. Misalignment condition between the TX coil and RX coil.

In this section, we analyzed the various conditions, such as the load variation, air gap variation, and misalignment condition. It can be summarized as follows.

(1) Variation in the load: X_{RX} is independent of the load.
(2) Variation in the air gap and occurrence of the misalignment: When the air gap changes or the misalignment occurs, the minimization condition of the leakage magnetic

field changes, i.e., the value of X_{RX} changes. It can be possible through a adaptive impedance matching network as explained [16].

3. Simulation and Experiment Verifications

In Section 3, we verify the proposed method through simulations and experiments.

3.1. Simulations of the Proposed Method Considering Various Cases

We verify the proposed method considering various cases, such as variation in the load and air gap. Figure 11 shows the simulation setup for the designed coil using ANSYS MAXWELL 3D electromagnetic (EM) solver. Table 2 shows the mechanical parameters of the TX and RX coils, and Table 3 shows the electrical parameters of the EM solver.

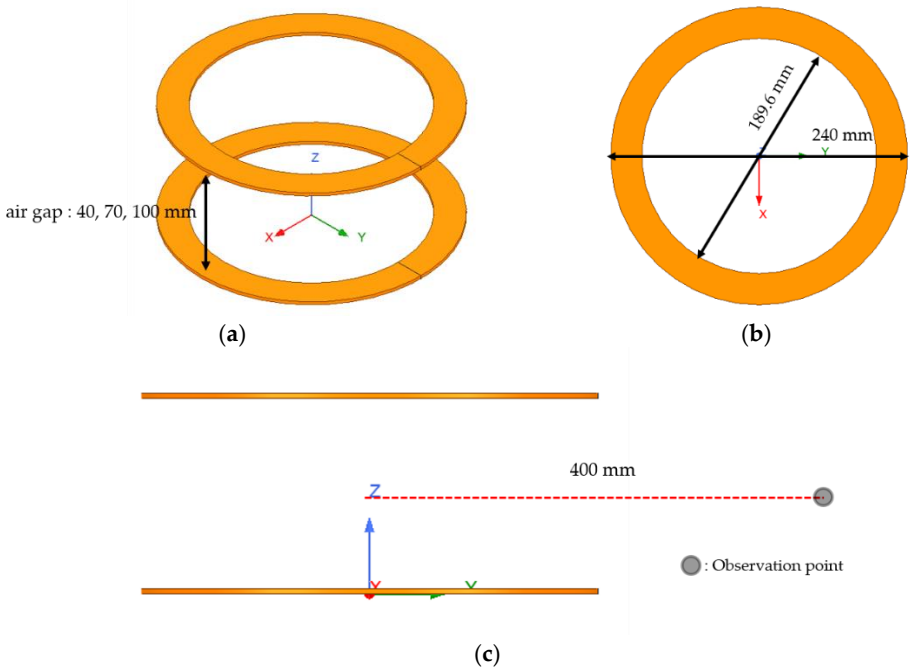

Figure 11. Setup for 3D EM solver: (**a**) aerial view; (**b**) top view; (**c**) observation point of the leakage magnetic field.

Table 2. Mechanical parameters of EM simulation.

Parameters	Value
Diameter of wire (TX, RX)	2.8 mm
Number of turns (TX, RX)	9 turns
Layer of coil (TX, RX)	1 layer

Table 3. Electrical parameters of TX and RX coils.

Parameters	Value
L_{TX}	31.94 µH
L_{RX}	31.94 µH
M_{TX-RX}	11.41 µH (air gap = 40 mm), 6.91 µH (air gap = 70 mm), 4.45 µH (air gap = 100 mm)

As shown in Table 3, we extracted three cases: air gap = 40, 70, and 100 mm, to verify the proposed method in various conditions. Figure 12 shows the circuit simulation setup, and Table 3 indicates the electrical parameters of the circuit simulation. As shown in

Figure 12, the WPT system is composed of the inverter, TX and RX coils, resonant capacitor, and full bridge rectifier.

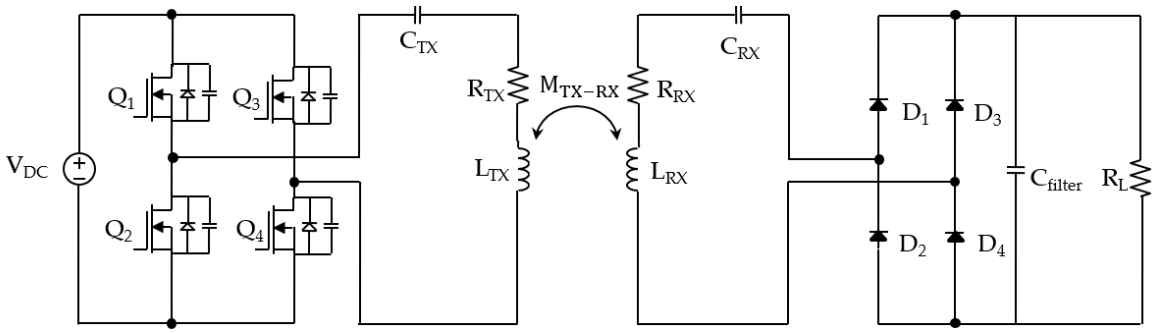

Figure 12. Setup for circuit simulation.

As shown in Table 4, the operating frequency of the inverter is 85 kHz, and C_{RX} changes depending on X_{RX}. The mutual inductance varies depending on the air gap, and the load resistor R_L varies to verify the proposed method in various cases.

Table 4. Electrical parameters of the circuit simulation.

Parameters	Value
f_o	85 kHz
L_{TX}/R_{TX}	31.94 µH/0.1 Ω (expected value)
C_{TX}	117.94 nF
L_{RX}/R_{RX}	31.94 µH/0.1 Ω (expected value)
C_{RX}	Variables (depending on the X_{RX})
M_{TX-RX}	11.41 µH (air gap = 40 mm), 6.91 µH (air gap = 70 mm), 4.45 µH (air gap = 100 mm)
R_L	3.08 Ω, 6.17 Ω, 12.34 Ω
P_{out}	50 W

In Equations (3) and (5), when X_{RX} is substituted by the condition in Equation (8), $\mathbf{I_{TX}}$ and $\mathbf{I_{RX}}$ can be expressed as in Equation (18).

$$\mathbf{I_{TX}} = \frac{\sqrt{{R_L}^2 + \left(\frac{N_{RX}}{N_{TX}}\left(\frac{d_{TX}}{d_{RX}}\right)^3 \omega_o M_{TX-RX}\right)^2}}{\omega_o M_{TX-RX}} I_{RX}\angle 0,\ \mathbf{I_{RX}} = I_{RX}\angle\left(-\frac{\pi}{2} - tan^{-1}\frac{\frac{N_{RX}}{N_{TX}}\left(\frac{d_{TX}}{d_{RX}}\right)^3 \omega_o M_{TX-RX}}{R_L}\right) \quad (18)$$

As shown in Equation (18), when N_{TX} and N_{RX} are the same, d_{TX} and d_{RX} are the same, the lower R_L, the higher operating frequency and M_{TX-RX}, and the phase difference between $\mathbf{I_{TX}}$ and $\mathbf{I_{RX}}$ is close to π, it is expected that the shielding performance increases. To verify the proposed method, we extracted the leakage magnetic field as shown in Figure 11c and the PTE through circuit simulation as shown in Figure 12 with the variation of X_{RX} through tuning the capacitor.

Figure 13 shows the simulation results when the load changes and the air gap is fixed to 70 mm. As expected, when the load resistor R_L increases, the phase difference between $\mathbf{I_{TX}}$ and $\mathbf{I_{RX}}$ becomes smaller, so the shielding performance gradually decreases. As shown in Figure 13, when the air gap is fixed to 70 mm, the shielding performances are 29.2%, 13.10%, and 3.61%, when the R_L is 3.08 Ω, 6.17 Ω, and 12.34 Ω, respectively

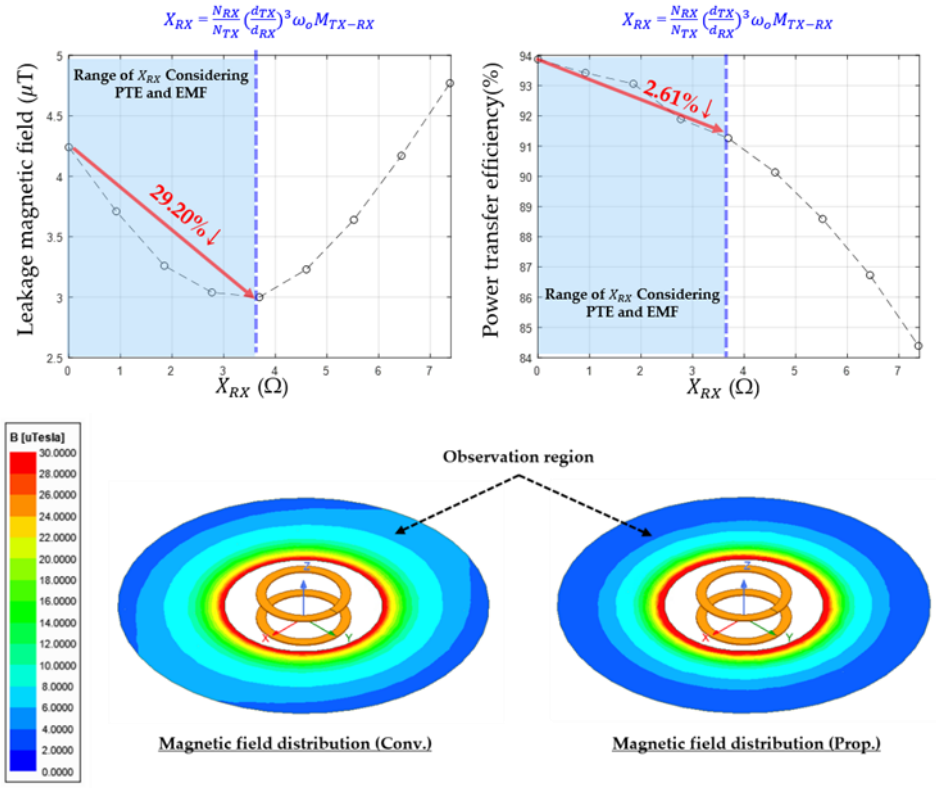

(**a**)

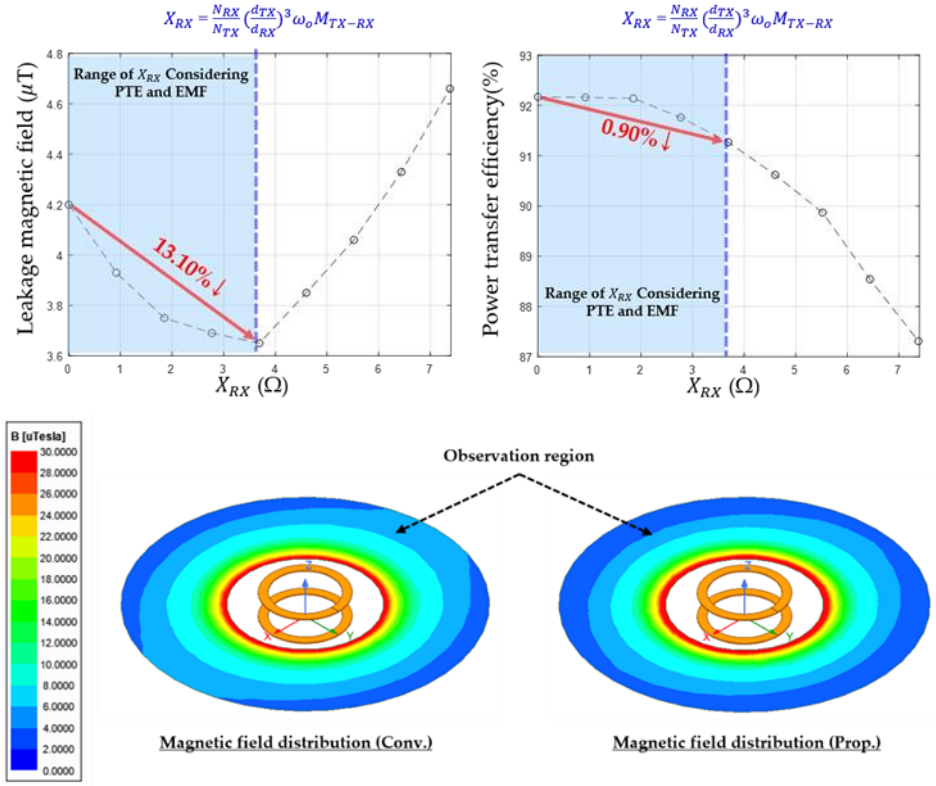

(**b**)

Figure 13. *Cont.*

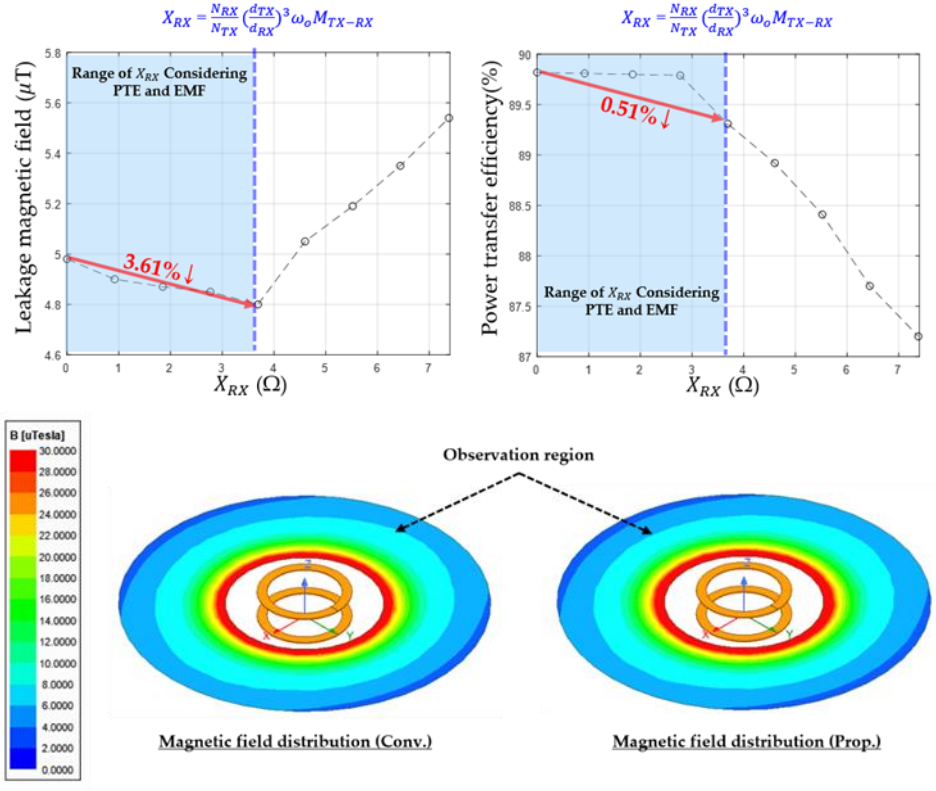

(**c**)

Figure 13. Simulation results (leakage magnetic field, PTE and magnetic field distribution) with variation of the load when the air gap is 70 mm: (**a**) 3.08 Ω; (**b**) 6.17 Ω; (**c**) 12.34 Ω.

In addition, Figure 14 shows the simulation results when the air gap changes and the load resistor R_L is fixed to 3.08 Ω. As expected, when the air gap increases, the phase difference between $\mathbf{I_{TX}}$ and $\mathbf{I_{RX}}$ become smaller, so the shielding performance gradually decreases also. As shown in Figure 14, when the load resistor is fixed to 3.08 Ω, the shielding performances are 49.60%, 29.20%, and 13.79%, when the air gap is 40 mm, 70 mm, and 100 mm, respectively.

To compare the proposed method and other shielding methods, we performed the simulation for the magnetic shielding method with metallic material, the reactive shielding method and the proposed method in condition Figure 13a. We extracted the leakage magnetic field at the observation point 400 mm from the center of the TX and RX coils and the PTE. Figure 15 shows the comparison of various shielding methods and the proposed method. As shown in Figure 15a, the shielding performance is highest when applying the passive shielding method, but when using the magnetic and metallic materials, the cost, size and weight may be increased. Meanwhile, the proposed method can reduce the magnetic field up to 49.60% without additional materials when compared to the conventional WPT system.

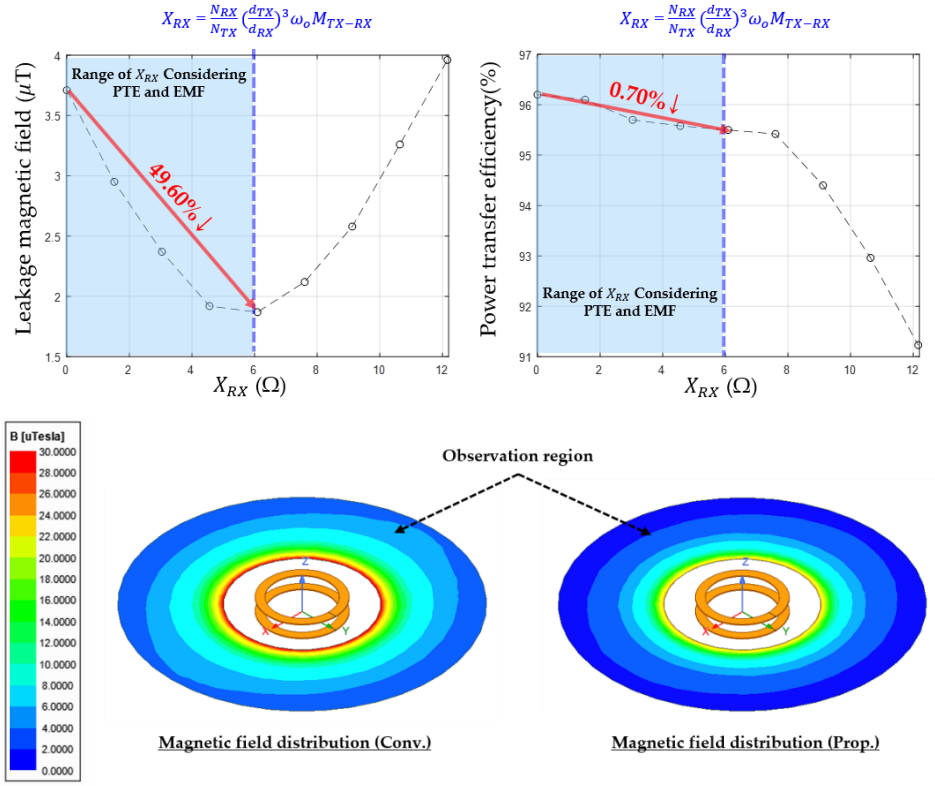

(**a**)

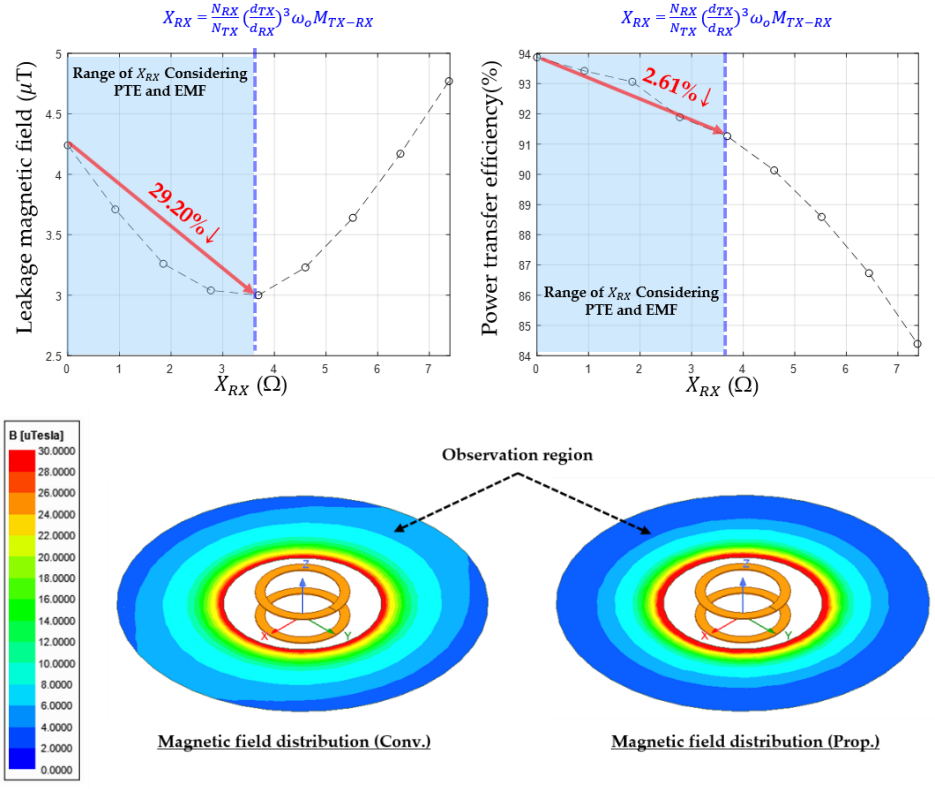

(**b**)

Figure 14. *Cont.*

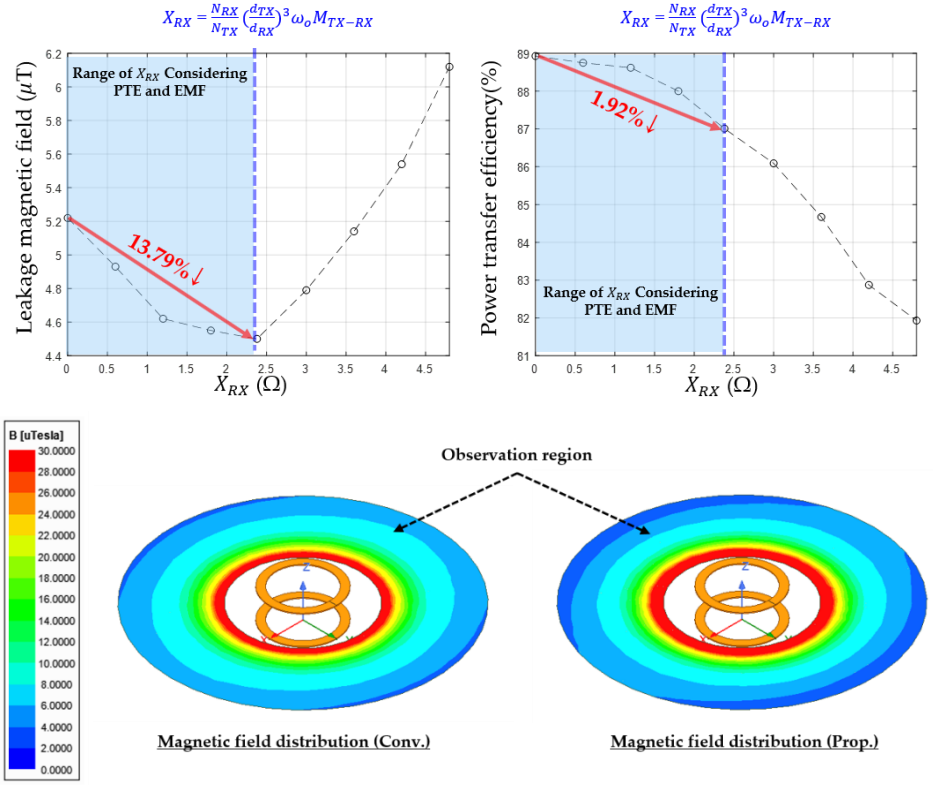

(**c**)

Figure 14. Simulation results (leakage magnetic field, PTE and magnetic field distribution) with variation of the air gap when the load is 3.08 Ω: (**a**) 40 mm; (**b**) 70 mm; (**c**) 100 mm.

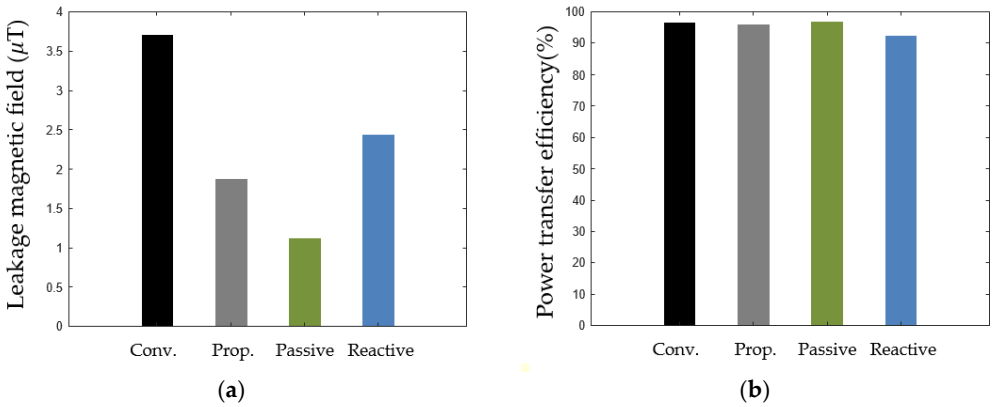

(**a**) (**b**)

Figure 15. Simulation results of various shielding methods and the proposed method: (**a**) leakage magnetic field level; (**b**) PTE.

3.2. Experiment Results

We verified the proposed method through the experiment. Figure 16 shows the setup for the experiment. We extracted the PTE using the DC power supply and the electronic load, and the leakage magnetic field using the ELT-400. Table 5 indicates the electrical parameters of the experiment. We set the operating frequency f_o as 85 kHz, and the output power P_{out} as 50 W. The capacitor of RX C_{RX} was set to 110.98 nF for the conventional WPT system, and 138.52 nF for the proposed WPT system.

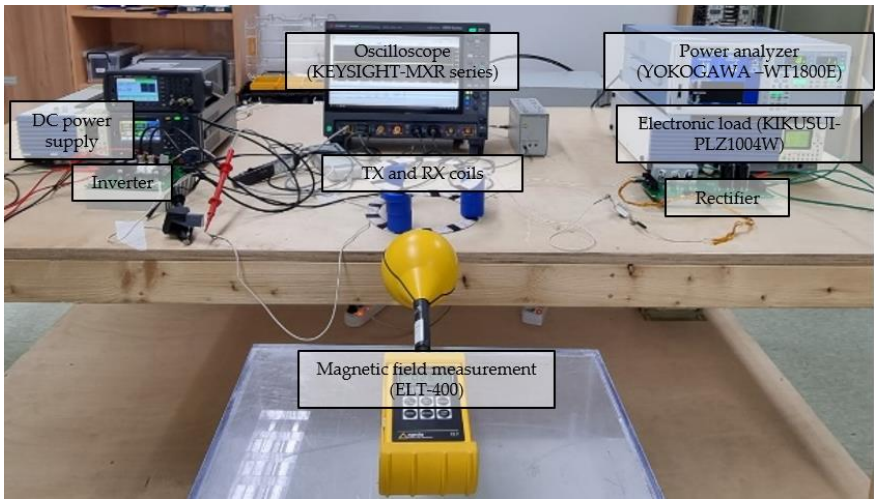

Figure 16. Setup for experimental verification.

Table 5. Electrical parameters for verification through experiment.

Parameters	Value
f_o	85 kHz
L_{TX}/R_{TX}	32.88 μH/0.08 Ω
C_{TX}	111.23 nF
L_{RX}/R_{RX}	32.52 μH/0.074 Ω
C_{RX}	110.98 nF (Conv.), 138.52 nF (Prop.)
M_{TX-RX}	6.75 μH (air gap = 70 mm)
R_L	2.98 Ω
P_{out}	50 W

Figure 17 shows the experiment results for the leakage magnetic field level and the PTE. As shown in Figure 17a, the leakage magnetic field level of the proposed method decreased from 4.72 μT to 3.19 μT when compared to the conventional WPT system, which is a decrease of 32.41%. In addition, as shown in Figure 17b, the PTE of the proposed method decreased by up to 2.44% when compared to the conventional WPT system. With reference to Equation (15), the PTC of the proposed WPT system is lower than that of the conventional WPT system. When employing the conventional and proposed system, the input DC voltage was 25 V and 30 V, respectively.

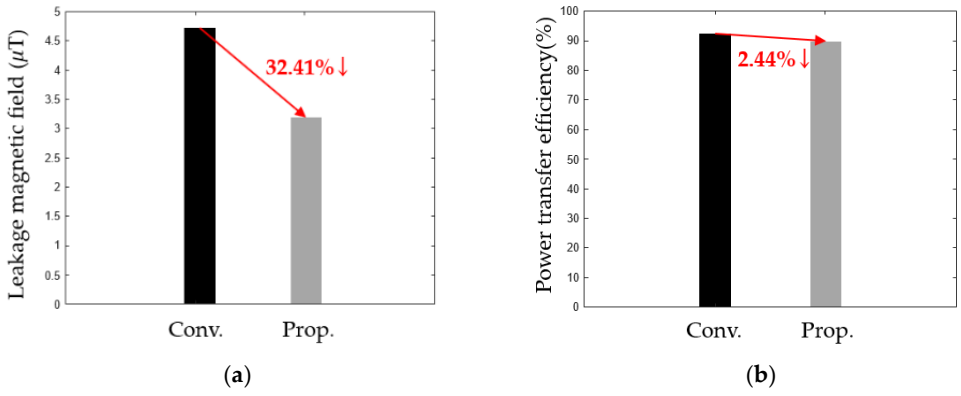

Figure 17. Experiment results: (**a**) leakage magnetic field level; (**b**) PTE.

In Section 3, we verified the proposed method through simulations and experiments. Through the simulations, the various cases, such as the variation of the load and air gap,

were verified, and experimental results show that the proposed method can reduce the leakage magnetic field level without any additional materials.

4. Conclusions

In this paper, we proposed a method for reducing the leakage magnetic field from the WPT system by controlling the phase difference between the TX coil current and RX coil current without any additional materials. The phase difference between the TX coil current and RX coil current can be controlled by tuning the matching capacitor of the RX coil.

The condition for minimizing the leakage magnetic field was derived mathematically, and the acceptable range for the selection of the matching capacitor of the RX coil was proposed.

Various cases, such as variation in the load, air gap, and the occurrence of misalignment were analyzed. Because the proposed method is independent of the load, it can be suitable for cases of changes in the load, such as using the DC–DC converter. In addition, when the air gap changes or a misalignment occurs, the resonant capacitor of the RX coil should be changed, and this is possible using the tunable matching network (TMN).

The simulations of the proposed method were performed in various cases, such as variation of the load, air gap, and the occurrence of misalignment. Through experiments, it was verified that the proposed method could reduce the leakage magnetic field by 32.41% while reducing the power transfer efficiency by 2.44%, without any additional materials. The proposed method can be suitable for the size-limited, weight-limited or cost-limited WPT systems because it does not require any additional coils, materials, or power sources.

Author Contributions: Conceptualization, S.W. and Y.S.; methodology, S.W., Y.S. and J.A.; validation, S.W., Y.S., C.L. and J.R.; formal analysis, S.W., H.K. and S.S.; investigation, S.W., S.L. and J.A.; writing—original draft preparation, S.W.; writing—review and editing, S.W., Y.S., C.L., J.R., J.A., J.M., S.S., S.L., H.K. and S.A.; supervision, S.A. All authors have read and agreed to the published version of the manuscript.

Funding: This work was supported by Institute of Information and Communications Technology Planning and Evaluation (IITP) grant funded by the Korean government (MSIT). (No. IITP-2020-0-00618, Development of commercialization technology for ultra small, high efficiency wireless charging for 1kW class robot).

Data Availability Statement: The data presented in this study are available on request from the corresponding author.

Acknowledgments: We would like to acknowledge the technical support from ANSYS Korea.

Conflicts of Interest: The authors declare no conflict of interest.

References

1. Patil, D.; McDonough, M.; Miller, J.; Fahimi, B.; Balsara, P.T. Wireless Power Transfer for Vehicular Applications: Overview and Challenges. *IEEE Trans. Transport. Electrif.* **2018**, *4*, 3–37. [CrossRef]
2. Li, S.; Mi, C.C. Wireless power transfer for electric vehicle applications. *IEEE J. Emerg. Sel. Top. Power Electron.* **2014**, *3*, 4–17.
3. Kim, D.; Kim, H.; Huang, A.; He, Q.; Zhang, H.; Ahn, S.; Zhu, Y.; Fan, J. Analysis and Introduction of Effective Permeability with Additional Air-Gaps on Wireless Power Transfer Coils for Electric Vehicle Based on SAE J2954 Recommended Practice. *Energies* **2019**, *12*, 4797. [CrossRef]
4. Park, J.; Kim, D.; Hwang, K.; Park, H.H.; Kwak, S.I.; Kwon, J.H.; Ahn, S. A Resonant Reactive Shielding for Planar Wireless Power Transfer System in Smartphone Application. *IEEE Trans. Electromagn. Compat.* **2017**, *59*, 695–703. [CrossRef]
5. Jeong, S.; Kim, D.-H.; Song, J.; Kim, H.; Lee, S.; Song, C.; Lee, J.; Song, J.; Kim, J. Smartwatch Strap Wireless Power Transfer System with Flexible PCB Coil and Shielding Material. *IEEE Trans. Ind. Electron.* **2019**, *66*, 4054–4064. [CrossRef]
6. Christ, A.; Douglas, M.; Nadakuduti, J.; Kuster, N. Assessing Human Exposure to Electromagnetic Fields from Wireless Power Transmission Systems. *Proc. IEEE* **2013**, *101*, 1482–1493. [CrossRef]
7. Monti, G.; Masotti, D.; Paolini, G.; Corchia, L.; Costanzo, A.; Dionigi, M.; Mastri, F.; Mongiardo, M.; Sorrentino, R.; Tarricone, L. EMC and EMI issues of WPT systems for wearable and implantable devices. *IEEE Electromagn. Compat. Mag.* **2018**, *7*, 67–77. [CrossRef]
8. Huang, L.; Zou, J.; Zhou, Y.; Hong, Y.; Zhang, J.; Ding, Z. Effect of Vertical Metal Plate on Transfer Efficiency of the Wireless Power Transfer System. *Energies* **2019**, *12*, 3790. [CrossRef]

9. Campi, T.; Cruciani, S.; Feliziani, M. Magnetic Shielding of Wireless Power Transfer Systems. In Proceedings of the 2014 International Symposium on Electromagnetic Compatibility, Tokyo, Japan, 12–16 May 2014; pp. 422–425.
10. Cruciani, S.; Campi, T.; Maradei, F.; Feliziani, M. Active Shielding Design and Optimization of a Wireless Power Transfer (WPT) System for Automotive. *Energies* **2020**, *13*, 5575. [CrossRef]
11. Son, S.; Woo, S.; Kim, H.; Ahn, J.; Huh, S.; Lee, S.; Ahn, S. Shielding Sensor Coil to Reduce the Leakage Magnetic Field and Detect the Receiver Position in Wireless Power Transfer System for Electric Vehicle. *Energies* **2022**, *15*, 2493. [CrossRef]
12. Shin, Y.; Park, J.; Kim, H.; Woo, S.; Park, B.; Huh, S.; Lee, C.; Ahn, S. Design Considerations for Adding Series Inductors to Reduce Electromagnetic Field Interference in an Over-Coupled WPT System. *Energies* **2021**, *14*, 2791. [CrossRef]
13. Song, C.; Kim, D.-H.; Yoon, K.; Kong, S.; Cho, Y.; Lee, S.; Jeong, S.; Song, K.; Hong, S.; Kim, J.; et al. Low EMI high-k Tightly-coupled Resonant Magnetic Field (TCR-HMF) Charger with Impedance Design for a 3-wheeler Vehicle. In Proceedings of the 2017 IEEE Wireless Power Transfer Conference (WPTC), Taipei, Taiwan, 10–12 May 2017; pp. 1–3.
14. Zhang, W.; Chris Mi, C. Compensation Topologies of High-Power Wireless Power Transfer Systems. *IEEE Trans. Vehic. Technol.* **2016**, *65*, 4768–4778. [CrossRef]
15. Shin, Y.; Woo, S.; Rhee, J.; Lee, C.; Kim, H.; Huh, S.; Park, B.; Ahn, S. Accurate Method for Extracting the Coupling Coefficient of an LCC-Series Wireless Power Transfer System. *IEEE Trans. Power Electron.* **2022**, *37*, 11406–11422. [CrossRef]
16. Lim, Y.; Tang, H.; Lim, S.; Park, J. An Adaptive Impedance-Matching Network Based on a Novel Capacitor Matrix for Wireless Power Transfer. *IEEE Trans. Power Electron.* **2014**, *29*, 4403–4413. [CrossRef]